International Journal of Nanomedicine

Dovepress
Taylor & Francis Group

Open Access Full Text Article

ORIGINAL RESEARCH

Yttrium Oxide Nanoparticles Affect Both Cognitive and Memory Function by Disrupting Copper Output in Neuronal Cells in a Rat Model

Manjia Zheng, Ziwei Chen, Jiling Xie, Qiyuan Yang, Minhua Mo, Liangjiao Chen

Department of Orthodontics, School and Hospital of Stomatology, Guangdong Engineering Research Center of Oral Restoration and Reconstruction & Guangzhou Key Laboratory of Basic and Applied Research of Oral Regenerative Medicine, Guangzhou Medical University, Guangzhou, People's Republic of China

Correspondence: Liangjiao Chen, Department of Orthodontics, School and Hospital of Stomatology, Guangdong Engineering Research Center of Oral Restoration and Reconstruction & Guangzhou Key Laboratory of Basic and Applied Research of Oral Regenerative Medicine, Guangzhou Medical University, No. 31 huangsha Road, Guangzhou, Guangdong, 510145, People's Republic of China, Email 2010686017@gzhmu.edu.cn

Background: The cerebral cortex is the foundation of cognitive function, and an imbalance in copper homeostasis in the cerebral cortex may cause cognitive and memory dysfunction. Metal exposure may disrupt copper (Cu) homeostasis in cells, leading to cognitive impairment. Yttrium oxide nanoparticles (Y_2O_3 NPs) are widely used in the biomedical field and have potential neurotoxicity. However, the influence of Y_2O_3 NPs on cognitive memory function in the brain is currently unclear.

Methods: The effects of Y_2O_3 NPs on cognitive and memory function were evaluated by rat behavioural experiments after intraperitoneal injection in a rat model. Subsequently, histological analysis was conducted on the cerebral cortex, and the Cu content and expression levels of cuproptosis-related proteins were detected both in vitro and in vivo. Finally, the copper output protein Cu transporting alpha polypeptide (ATP7A) was screened and detected at the mRNA and protein levels. Plasmid transfection experiments further confirmed that Y_2O_3 NPs mediate disordered Cu output through ATP7A.

Results: Y_2O_3 NP exposure induced cognitive and memory dysfunction in rats. This effect was related to the disruption of copper homeostasis in neuronal cells caused by Y_2O_3 NPs, which induced cuproptosis. Further research revealed that Y_2O_3 NPs downregulate ATP7A expression, thus disrupting copper output and inducing cuproptosis.

Conclusion: Y_2O_3 NPs induce cognitive and memory dysfunction by mediating the disruption of copper output in neuronal cells, revealing the toxicity of Y_2O_3 NPs to neurons. These findings contribute to their safe application in the biomedical field.

Keywords: Yttrium oxide nanoparticles, neurotoxicity, neuronal cells, copper homeostasis, cuproptosis

Introduction

Cognitive impairment refers to deficits in learning and memory caused by abnormal learning, memory, and cognitive judgement functions in the brain.[1] The cerebral cortex is the foundation of cognitive function, and structural and functional abnormalities in the cerebral cortex caused by external factors may lead to cognitive impairment. Common environmental pollutants, such as heavy metals, pesticides, and microplastics, are neurotoxic and pose risks of cognitive and memory impairments. Among them, exposure to nanomaterials in the environment may lead to cognitive and memory impairments. For example, nanoplastics affect hippocampal neurogenesis, leading to impaired cognitive and memory function.[2] Exposure to manganese nanoparticles can affect the basal ganglia and induce cognitive dysfunction, leading to Parkinson's disease.[3]

Cu is an important trace element and is essential for synapse formation, neurotransmitter activation and other neuronal cell functions.[4] The dysregulation of neuronal Cu homeostasis may lead to cognitive and memory impairments. For example, the dysregulation of neuronal Cu homeostasis can increase Aβ plaque deposition and oxidative damage to neuronal cells, promoting the development of Alzheimer's disease.[5] Metal exposure may disrupt Cu homeostasis in cells,

Received: 6 January 2025
Accepted: 12 April 2025
Published: 6 May 2025

Graphical Abstract

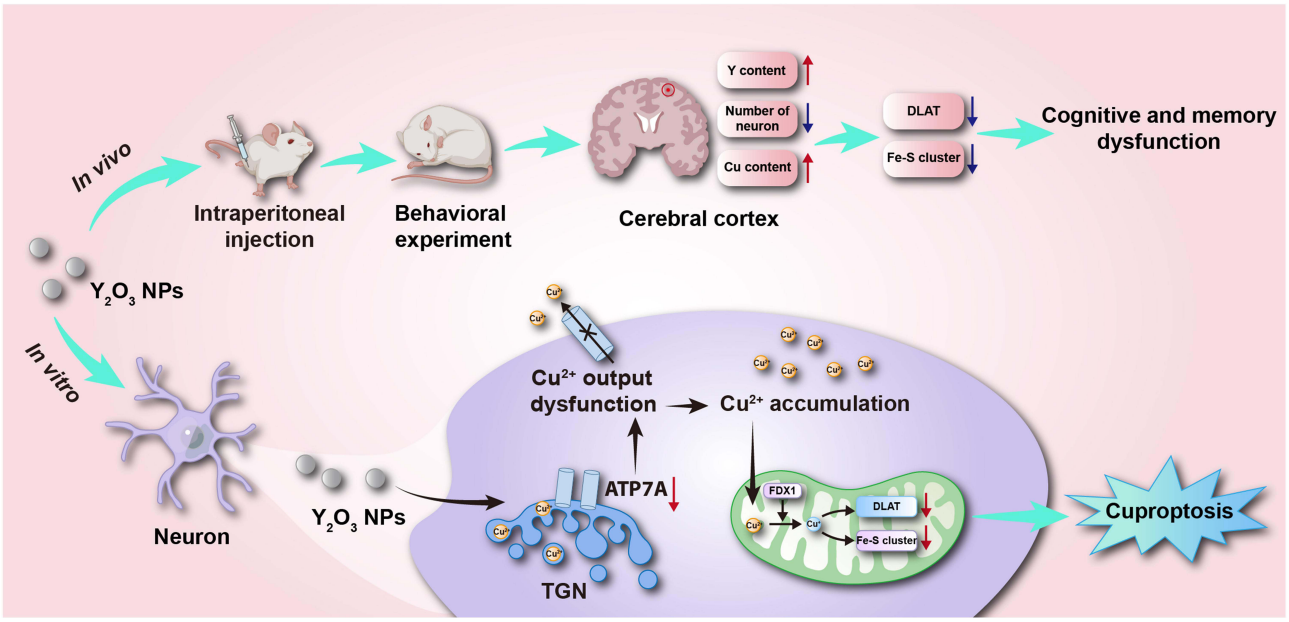

leading to cognitive impairment and the development of neurodegenerative diseases. Rare earth elements have the potential to induce memory impairment and anxiety-like depression behaviour in mice.[6] Yttrium (Y) was the first rare earth element to be discovered, and the global reserves and consumption of Y are enormous.[7] Y_2O_3 NPs are widely used in fields such as bioimaging, materials science, and inorganic compound synthesis.[8] With the widespread application of Y_2O_3 NPs, the risk of their release into the environment has increased, potentially resulting in adverse effects on human health.

Experimental results have shown that Y_2O_3 NPs are cytotoxic and pose a threat to human health. Andelman et al studied the effects of Y_2O_3 NP exposure on human fibroblasts and observed concentration-dependent cytotoxicity.[9] Selvaraj et al reported that Y_2O_3 NPs cause apoptosis, necrosis, and DNA damage in human embryonic kidney cells, leading to genetic toxicity.[10] Another study showed that intravenous injection of Y_2O_3 NPs leads to the apoptosis of mouse bone marrow stromal cells and induces bone destruction.[11] Notably, Y^{3+} can induce neuronal cell apoptosis in rats.[12] These findings suggest that Y_2O_3 NPs have potential neurotoxicity.

The blood–brain barrier protects neuronal cells from external factors and regulates the internal environment of the central nervous system. Y_2O_3 NPs can pass through the blood–brain barrier and be deposited in the brain through oral administration and tail injection in rats.[13,14] A previous study revealed that Y_2O_3 NPs cause cognitive and memory dysfunction in the brain; however, the specific mechanism is still unclear. This research investigates the influence of Y_2O_3 NP exposure on cognitive memory function and neuronal cells in rats and explores the potential mechanisms involved. By shedding light on the possible damage to neuronal cells caused by Y_2O_3 NPs, this study adds to our knowledge of the neurotoxicity of Y_2O_3 NPs and may help advance their use in biomedicine.

Materials and Methods

Characterization of Yttrium Oxide Nanoparticles

Y_2O_3 NP powder was obtained from Aladdin (Shanghai, China). The surface morphology and particle diameter of the Y_2O_3 NPs were evaluated by transmission electron microscopy (TEM) (Hitachi-7800, Japan). The elemental composition

of the Y_2O_3 NPs was analysed via energy dispersive spectroscopy (EDS) (SwiftED3000, Japan). A Zetasizer Nano-ZS90 (Malvern, UK) was used to measure the zeta potential of the Y_2O_3 NPs.

In vivo Studies Using a Rat Model

Animal Treatment and Behaviour Tests

Sixteen healthy male Sprague–Dawley (SD) rats, weighing 140–160 g and aged 4–6 weeks, were purchased from Guangdong Vital River Laboratory Animal Technology Co., Ltd. (Guangzhou, China). The rats were housed under a 12-hour light/dark cycle. The Chinese National Animal Ethics Committee approved these animal experiments. Approval was provided by Guangdong Huawei Testing Co., Ltd. (No. 202302002). The animal experiments were carried out in compliance with *Laboratory Animals—Guidelines for the Ethical Review of Animal Welfare* (GB/T 35892–2018) and the *Guide for the Care and Use of Laboratory Animals*. After 5 days of adaptation, four groups of rats were randomly assigned to the following groups: control group (saline), 50 mg/kg Y_2O_3 NP group, 100 mg/kg Y_2O_3 NP group, and 200 mg/kg Y_2O_3 NP group. Y_2O_3 NPs were dispersed in distilled water and sonicated for 1 h to prepare a Y_2O_3 NP suspension, which was injected intraperitoneally daily into the rats for 14 consecutive days. The rats were weighed every two days.

To evaluate the influence of Y_2O_3 NPs on spatial memory and cognitive performance, behavioural tests were conducted in rats (n=4) after 14 days of intraperitoneal injection of Y_2O_3 NPs. After the behaviour tests, euthanasia was performed under anaesthesia, and the brain of each rat was perfused and weighed to calculate the brain organ coefficient.

Open Field Test

The rats were placed in the centre of a square room and left to roam freely for 5 min. Rat movements were tracked with a camera (Xinruan, Shanghai, China). After each experiment, the chamber was thoroughly cleaned with 75% ethanol to ensure the removal of any smells prior to drying. Software was used to record and analyse the total distance travelled, movement speed, and percentage of movement time.

Morris Water Maze Test

The Morris water maze (MWM) test apparatus included a round pool of water (2.0 m × 0.8 m) and a platform 2 cm underwater. The pool was filled with water (25 ± 1 °C) and divided into four quadrants. The rats were trained for 4 days in positioning navigation, starting from different quadrants and performing 4 trials, with 90s per trial to determine the location of the escape platform. Spatial probe tests were performed on the 5^{th} day. After the platform was removed, the rats were given 60s to swim freely. The number of times the rats crossed the former platform location and the time spent and the travel distance in the target quadrant were recorded. Throughout the training and testing periods, a ceiling-mounted tracking system (Hua Wei Biotechnology Company; Guangzhou, China) was utilized for automated data recording purposes.

Determination of Yttrium and Copper Contents

One milligram of frozen cerebral cortex tissue was digested with concentrated ultrapure grade nitric acid and H_2O_2. The Y content was quantitatively measured via inductively coupled plasma–mass spectrometry (ICP–MS) (Thermo Fisher Scientific, MA, USA).

Cu in the cerebral cortex tissue was quantified using a Cu colorimetric assay kit (E-BC-K300-M; Elabscience, Wuhan, China). The cerebral cortex tissue was homogenized with distilled water and centrifuged to obtain the supernatant for testing. A portion of the supernatant was used to determine the protein concentration. The appropriate reagents were mixed with each sample in accordance with the kit instructions, and the samples were incubated at 37 °C for 5 min. A microplate reader (Bio-Tek, USA) was used to measure the optical density at 580 nm. The Cu content was calculated on the basis of the optical density value and protein concentration.

Histopathological Studies

The brain was fixed in paraffin and cut into slices. The brain slices were deparaffinized in stages with alcohol (100%, 95%, and 90%, 80%), followed by haematoxylin and eosin (HE) staining. The sections were mounted on glass slides, and then the cortical areas of the brain were examined under an upright fluorescence microscope.

Immunohistochemistry (IHC) was used to evaluate the number of neuronal cells and cuproptosis. To determine the number of neuronal cells, immunohistochemistry was performed using an antibody against NeuN (1:10000, Proteintech, USA). The expression of dihydrolipoamide S-acetyltransferase (DLAT), iron-sulfur (Fe-S) cluster proteins, and ATP7A was evaluated using antibodies against recombinant ferredoxin 1 (FDX1) (1:200, ABclonal, China), DLAT (1:100, Proteintech, USA), aconitase 2 (ACO2) (1:100, Proteintech, USA), lipoyl synthase (LIAS) (1:100, Proteintech, USA), succinate dehydrogenase complex, subunit B (SDHB) (1:200, Proteintech, USA) and ATP7A (1:100, Abmart, China). Using a pressure cooker set to a high temperature, antigen repair was carried out in citric acid buffer (Beyotime, Shanghai, China). The brain slices were incubated with anti-FDX1, anti-DLAT, anti-ACO2, anti-LIAS, anti-SDHB and anti-ATP7A antibodies overnight at 4 °C after blocking endogenous peroxidase activity for 1 h. Following a 1-h incubation period with HRP-conjugated goat anti-rabbit IgG (H+L) (1:150, Beyotime, China), the sections were subjected to IHC staining using a DAB kit (Biolab, China). Positively stained (brown) cerebral cortex regions were imaged, and cell counting was performed using ImageJ software.

Observation of Cellular Ultrastructure by Transmission Electron Microscopy

After being fixed for 24 h with a 2.5% glutaraldehyde fixative solution (G1102-100ML, Servicebio, Wuhan, China), the brain cortical tissue (2 mm × 2 mm) was dried and embedded in Epon resin. The tissue was then sliced into ultrathin tissue sections, which were then placed on grids. The ultrastructure was observed using an H7800 transmission electron microscope (Hitachi, Tokyo, Japan).

In vitro Studies Using a Neuronal Cell Model

Cell Culture and Cell Viability Assay

PC12 (highly differentiated) cells were obtained from Procell Life Science & Technology Co., Ltd., Wuhan, China (CL-0481), and cultured in RPMI 1640 medium (C11875500BT, Gibco, Shanghai, China) supplemented with 10% FBS (164210, Pricella, Wuhan, China) and 1% penicillin/streptomycin (G4003, Servicebio, Wuhan, China) in a 5% CO_2 incubator at 37 °C. In accordance with the experimental design, the cells were passaged in a new culture bottle at a ratio of 1:2 or 1:3, and the cells chosen for further studies were those in the logarithmic growth phase.

A Cell Counting Kit-8 (B34304, Selleck, Shanghai, China) was used to measure the viability of the cells. Y_2O_3 NPs were added to 96-well plates containing 5×10^3 cells at different doses (0, 0.1, 1, 5, 10, or 100 μg/mL) for 48 hours in growth medium containing Cu (40 μM CuCl2). Following the addition of 10 μL of Cell Counting Kit-8 (CCK-8) solution to each well, the cells were incubated for 2 h at 37 °C. A microplate reader (Bio-Tek, USA) was used to measure the absorbance at 450 nm. Each group had three replicate wells with at least three independent replicates.

Determination of Yttrium and Copper Contents

PC12 cells (5×10^5) were digested with concentrated ultrapure grade H_2O_2. The Y content was quantitatively ascertained via inductively coupled plasma–mass spectrometry (ICP–MS) (Thermo Fisher Scientific, MA, USA).

The intracellular copper concentration was determined via a Cu colorimetric test kit (E-BC-K775-M, Elabscience, Wuhan, China). Following a 48-hour control and Y_2O3 NP treatment period, PC12 cells ($1x10^7$) were treated with lysis buffer and lysed for 10 minutes on ice. The supernatant was collected by centrifugation for determination of the Cu content. A portion of the supernatant was used to measure the protein concentration. The appropriate reagents were mixed with each sample in accordance with the kit instructions. A microplate reader (Bio-Tek, USA) was used to measure the optical density at 580 nm after the samples had been incubated for five minutes at 37 °C. Finally, the Cu content was calculated on the basis of the optical density value and protein concentration.

Immunofluorescence Staining

The expression of DLAT, Fe-S cluster proteins, and ATP7A was assessed using antibodies against DLAT (1:100, Proteintech, USA), FDX1 (1:200, ABclonal, China), ACO2 (1:100, Proteintech, USA), LIAS (1:100, Proteintech, USA), and ATP7A (1:100, Abmart, China). The samples were incubated with a primary antibody overnight at 4 °C after being treated for 1 h with QuickBlock™ Blocking Buffer for Immunol Staining (Beyotime, Shanghai, China). This was followed by an incubation period of 1 h with CoraLite 488-conjugated AffiniPure goat anti-rabbit IgG (H+L) (1:200, Proteintech, USA). Finally, the samples were incubated with 4,6-diamino-2-phenyl indole (DAPI) staining solution (Beyotime, China), after which immunofluorescence (IF) imaging was conducted.

RNA-Seq Assay and Reverse Transcription Quantitative Polymerase Chain Reaction (RT–qPCR)

Using an E ZB Cell/Tissue Total RNA Isolation Kit (EZBioscience, US), total RNA was extracted from PC12 cells. A NanoDrop spectrophotometer (Thermo Scientific, USA) was used to measure the quality and concentration of each sample. According to the manufacturer's instructions, a reverse transcription kit (Accurate Biology, China) was utilized. The SYBR Green Pro Taq HS Premix qPCR Kit (ABclonal, Wuhan, China) was used to conduct quantitative PCR (qPCR). The ΔΔCt method was used to normalize the mRNA expression levels to the level of glyceraldehyde-3-phosphate dehydrogenase (GAPDH). Table S1 contains a list of all the primer sequences utilized for PCR amplification.

Western Blot

RIPA lysis buffer (Beyotime, Shanghai, China) supplemented with PMSF (Beyotime, Shanghai, China) was used to lyse the collected cultured cells and cerebral cortex tissues for 30 min. Afterwards, the samples were centrifuged for 30 min at 4 °C at 12,000 rpm. A BCA protein assay kit (Beyotime, Shanghai, China) was used to measure the protein concentration. The protein was electrophoretically transferred to 0.45 μm PVDF membranes (Millipore, Carlsbad, Ireland) at 400 mA constant current for 1 h after 10–20 μg of protein was loaded onto 7.5–12.5ED% Bis-Tris SDS–polyacrylamide gels. The membrane was then blocked for 1 h with 5% skim milk powder (Beyotime, Shanghai, China). The membranes were incubated with antibodies against DLAT (1:2000, Proteintech, USA), FDX1 (1:1000, ABclonal, China), recombinant protein 1 (POLD1) (1:3000, Abcam, UK), ACO2 (1:2000, Proteintech, USA), LIAS (1:3000, Proteintech, USA), SDHB (1:3000, Proteintech, USA), ATP7A (1:1500, Abmart, China), GAPDH (1:5000, Proteintech, USA) and β-actin (1:5000, Proteintech, USA) overnight at 4 °C. Then, HRP-conjugated goat anti-rabbit IgG (H+L) (1:2000, Proteintech, USA) was added to the PVDF membrane, and protein bands were visualized via ultrahigh-sensitivity ECL (HY-K1005, EpiZyme, China).

Plasmid Transfection

A 6-well plate was seeded with PC12 cells (1×10^5 cells/mL), and then 2 mL of RPMI 1640 medium was added. To transfect the pcDNA3.1(+)-Flag-ATP7A overexpression plasmid, Lipofectamine 3000 transfection reagent (Thermo Fisher, USA) was used in Opti-MEM (Thermo Fisher, USA). The cells were incubated for 48 h after the medium was changed to RPMI 1640 medium after 6 h.

Statistical Analysis

For every data set, at least three independent replicates were conducted. Using GraphPad Prism software, unpaired t tests or a normal one-way ANOVA were used to analyse the results, which are shown as the means ± standard deviations (SDs). The threshold for statistical significance was set at $P<0.05$.

Results

Characterization of Yttrium Oxide Nanoparticles

TEM micrographs revealed that the Y_2O_3 NPs were rod-shaped (Figure 1A). The diameter of the Y_2O_3 NPs measured via ImageJ analysis was approximately 35 nm (Figure 1B). EDS analysis revealed that the elemental composition of the

 https://doi.org/10.2147/IJN.S515951

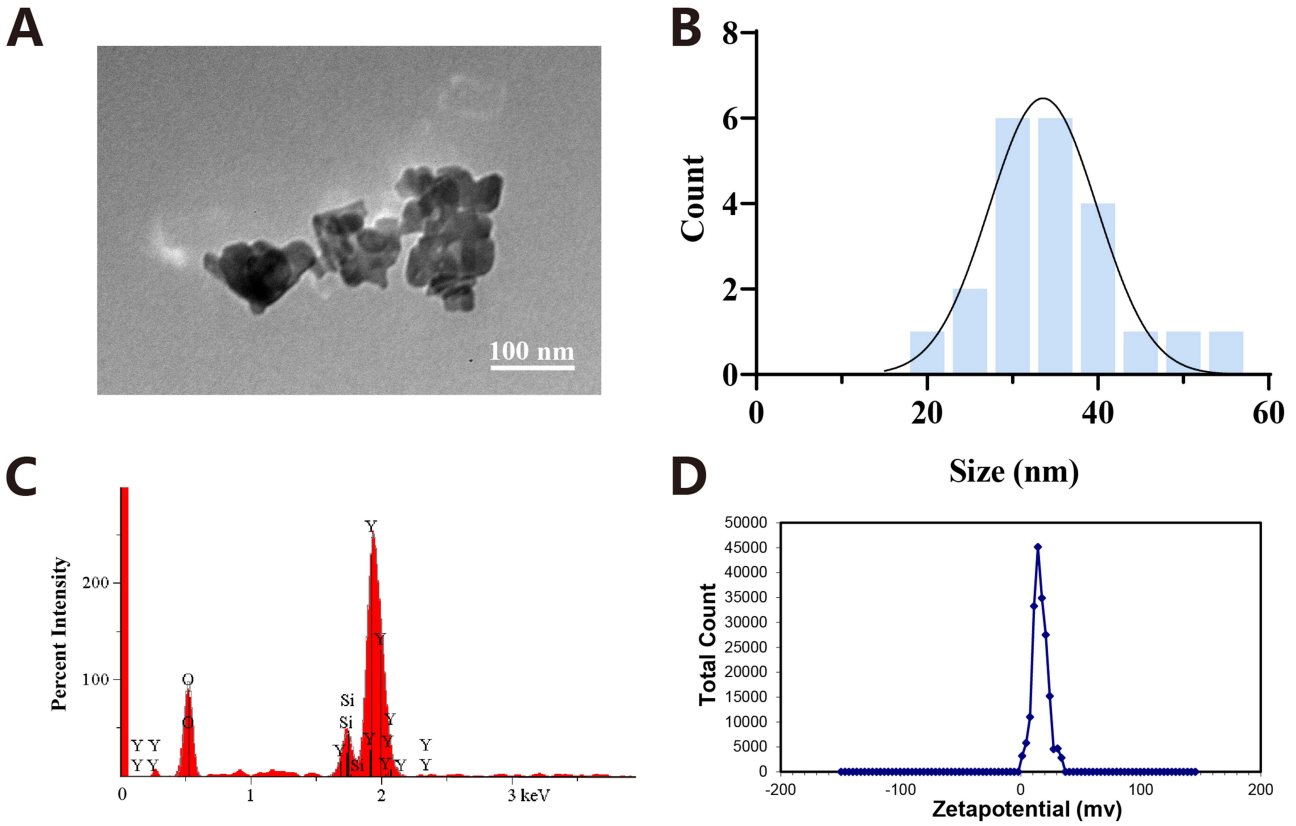

Figure 1 Characterization of the Y_2O_3 NPs. (**A**) TEM micrograph of the Y_2O_3 NPs. (**B**) Particle size distribution diagram of the Y_2O_3 NPs. (**C**) Elemental analysis of the Y_2O_3 NPs. (**D**) Zeta potential of the Y_2O_3 NPs.

Y_2O_3 NPs was mainly Y and O (Figure 1C). The zeta potential of the Y_2O_3 NPs was 16.2 mV (Figure 1D), indicating a positively charged surface.

Yttrium Oxide Nanoparticles Impair Cognitive Memory Capacity and Motor Function in Rats

The neural function of rats exposed to Y_2O_3 NPs for 14 days was assessed through animal behavioural experiments. Figure 2A shows the in vivo experimental scheme. To assess the influence of the Y_2O_3 NPs on motor function in rats, the open field (OF) test was used to observe spontaneous movement. Compared with those in the control group, the total distance travelled and the mean velocity were lower in the 50 mg/kg, 100 mg/kg and 200 mg/kg Y_2O_3 NP groups (Figure 2B and C). The percentage of mobility time was decreased in the 100 mg/kg and 200 mg/kg Y_2O_3 NP groups (Figure 2D). The MWM test was then used to evaluate the influence of the Y_2O_3 NPs on cognitive and memory performance in rats. There was a decrease in the number of platform crossings and the time spent and travel distance in the target quadrant in the 100 mg/kg and 200 mg/kg Y_2O_3 NP groups, but there was no decrease in the number of platform crossings in the 50 mg/kg Y_2O_3 NP group (Figure 2E–G). Figure 2H displays representative swimming trajectories of the rats in the MWM test. In contrast to those in the control group, the swimming trajectories of the Y_2O_3 NP groups were irregular. These results indicate that Y_2O_3 NP exposure impairs motor function and cognitive memory capacity in rats.

Yttrium Oxide Nanoparticle Exposure Leads to Copper Accumulation and Neuronal Cell Death in the Cerebral Cortex of Rats

After 14 days of Y_2O_3 NP intraperitoneal injection, the brain organ coefficient of the rats in the Y_2O_3 NP group significantly increased, indicating that the brain may have undergone pathological changes (Figure 3A). ICP–MS was used to assess the

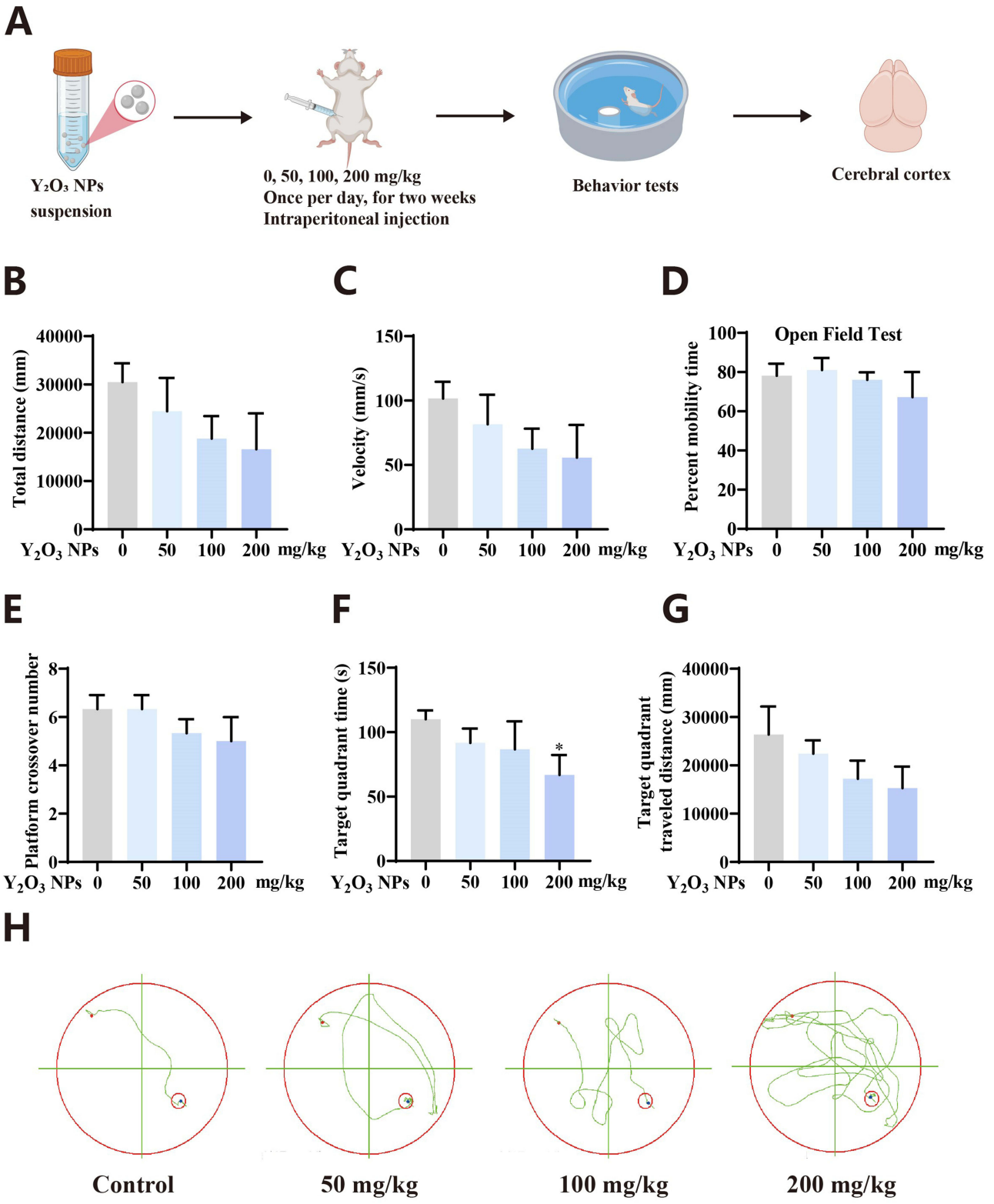

Figure 2 Y_2O_3 NPs impair cognitive memory capacity and motor function in rats. (**A**) Scheme for the in vivo experiments. (**B**) The total distance travelled in the OF test. (**C**) The mean velocity in the OF test. (**D**) The percentage of time spent mobile in the OF test. (**E**) The number of platform crossings in the probe trial. (**F**) Time spent in the target quadrant. (**G**) Travel distance in the target quadrant. (**H**) Representative swimming trajectories of the rats in the MWM test. The results are shown as the means ± SDs. * $P<0.05$, n=3.

https://doi.org/10.2147/IJN.S515951

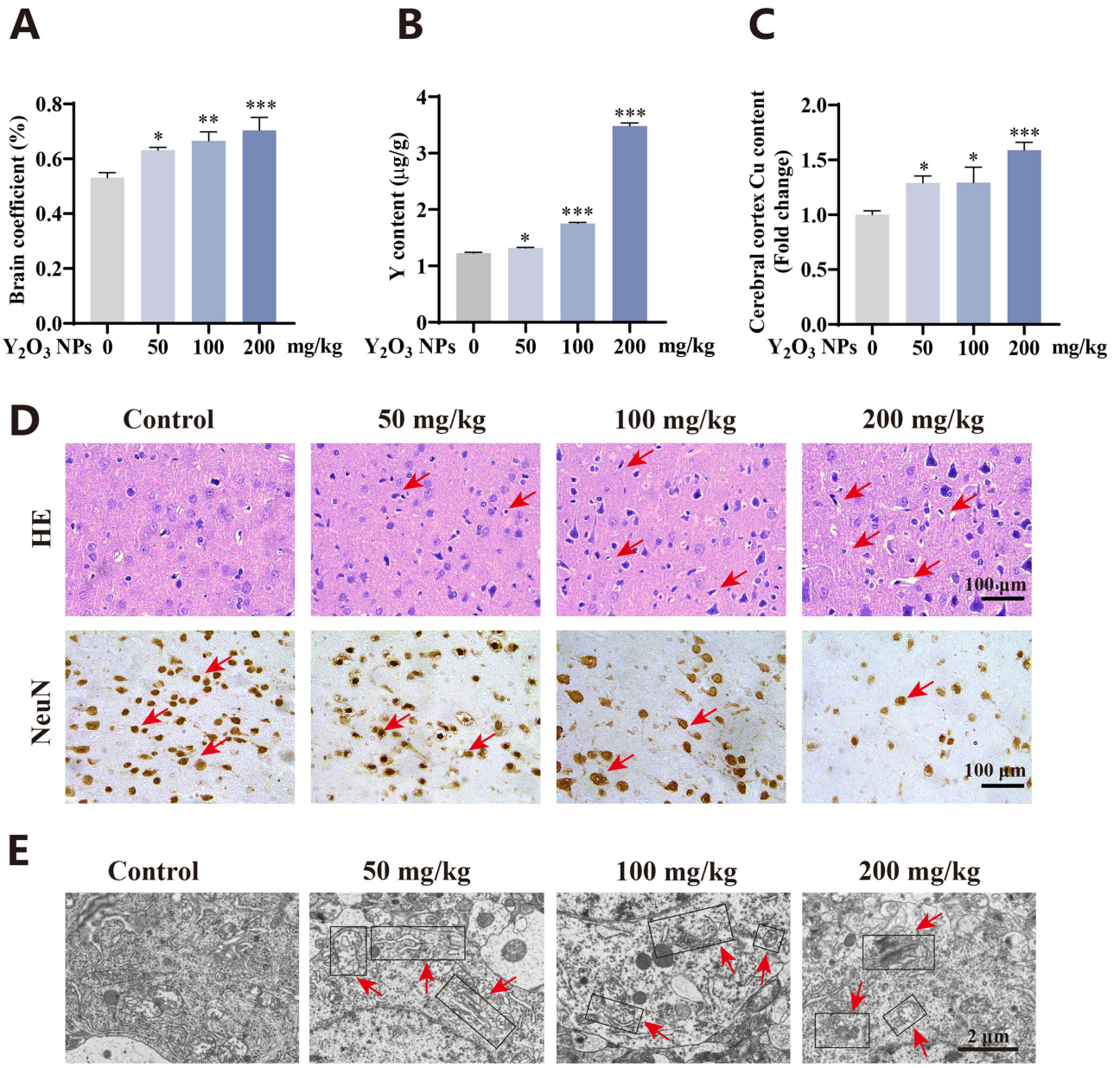

Figure 3 Y_2O_3 NP exposure leads to Cu accumulation and neuronal cell death in the cerebral cortex of rats. (**A**) Brain organ coefficient after exposure to the Y_2O_3 NPs. (**B**) Y content in the cerebral cortex of the rats after exposure to the Y_2O_3 NPs. (**C**) Cu content in the cerebral cortex of rats after exposure to the Y_2O_3 NPs. (**D**) HE staining and IHC staining of NeuN in the rat cerebral cortex after exposure to the Y_2O_3 NPs. The red arrows indicate condensed cytoplasm and nuclear pyknosis with intense staining. The brown-stained area of the nucleus indicates the positive IHC staining area (red arrows). (**E**) TEM micrographs of neuronal cells in the cerebral cortex after exposure to the Y_2O_3 NPs. The boxed areas indicated by the red arrows represent structural disruption of the mitochondria, endoplasmic reticulum, and Golgi apparatus. The results are shown as the means ± SDs. *P<0.05, **P<0.01, and ***P<0.001.

Y content in the cerebral cortex, and the results revealed an increase in the Y content in the Y_2O_3 NP group (Figure 3B). To investigate whether Y_2O_3 NPs affect Cu homeostasis in the brain, Cu levels were measured in the cerebral cortex. The results revealed that in the 50 mg/kg group, Y_2O_3 NPs increased Cu levels in the cerebral cortex (Figure 3C). Figure 3D shows the morphologic changes in the cerebral cortex observed by HE staining. In contrast to that in the control group, neuronal cell death in the Y_2O_3 NP group was more extensive, characterized by cytoplasmic condensation and nuclear hyperchromatic pyknosis (indicated by red arrows). The number of neuronal cells in the cerebral cortex was determined via NeuN IHC staining (Figure 3D). The brown-stained area of the nucleus indicates the positive staining area, and the results revealed that the number of neuronal cells significantly decreased in the 100 mg/kg Y_2O_3 NP group. Ultrastructural changes in neuronal cells in the

cerebral cortex were observed by TEM (Figure 3E). In contrast to those in the control group, the destruction of organelles in the 100 and 200 mg/kg Y_2O_3 NP groups was evident, characterized by mitochondrial swelling, cristae rupture, Golgi apparatus and rough endoplasmic reticulum dilation, and an unclear structure. The degree of organelle destruction was dose dependent. These results indicate that Y_2O_3 NPs can be deposited in the rat cerebral cortex, leading to Cu accumulation and neuronal cell death.

Yttrium Oxide Nanoparticles Induce Cuproptosis in the Rat Cerebral Cortex

We investigated whether Y_2O_3 NPs induce cuproptosis in neuronal cells in vivo. The expression of proteins related to cuproptosis in the rat cerebral cortex was observed by IHC staining. The brown-stained area in the cytoplasm was considered the positive area. Downregulated cuproptosis-related protein expression in neuronal cells of the cerebral cortex was observed in the 100 mg/kg and 200 mg/kg Y_2O_3 NP groups (Figure 4A). According to Western blot analysis, the levels of DLAT, ACO2, LIAS and SDHB were decreased in the 100 mg/kg or 200 mg/kg Y_2O_3 NP groups, whereas the levels of FDX1 and POLD1 were decreased only in the 200 mg/kg Y_2O_3 NP group (Figure 4B). These results indicate that Y_2O_3 NPs induce cuproptosis in neuronal cells in vivo.

Yttrium Oxide Nanoparticles Induce Neuronal Cell Cuproptosis

To investigate how Y_2O_3 NPs cause neuronal cell death, PC12 cells were treated with Y_2O_3 NPs. Adding exogenous Cu (40 μM) to the culture medium simulated the Cu environment in the brain, and this concentration of Cu had no effect on cell viability (Figure S1). The minimum toxic concentration of Y_2O_3 NPs was determined using the CCK8 assay (Figure 5A). Y_2O_3 NPs decreased the viability of PC12 cells in a concentration-dependent manner, with a notable decrease starting at 5 μg/mL. Therefore, we used 5 μg/mL Y_2O_3 NPs to treat PC12 cells in subsequent experiments. ICP–MS revealed an increase in the Y content of PC12 cells in the Y_2O_3 NP group (Figure 5B). To determine whether Y_2O_3 NPs had an effect on Cu homeostasis in PC12 cells, Cu levels were measured (Figure 5C). The Cu ion carrier elesclomol (ES) was used as a positive control and caused copper accumulation in cells and induced cuproptosis. Y_2O_3 NPs increased the intracellular Cu concentration, similar to the effect of ES. The protein expression of Caspase-3 and GPX4 revealed that the major mode of death of PC12 cells induced by Y_2O_3 NPs was not apoptosis or ferroptosis (Figure 5D). Excessive intracellular Cu accumulation can lead to cuproptosis, indicating that the disruption of Cu homeostasis caused by Y_2O_3 NPs may induce cuproptosis in PC12 cells. Western blot analysis of DLAT and Fe-S cluster proteins (FDX1, POLD1, ACO2, LIAS and SDHB) revealed that Y_2O_3 NPs reduced the expression of proteins related to cuproptosis in PC12 cells, which was consistent with the trend in the ES treatment group (Figure 6A). IF analysis confirmed that Y_2O_3 NPs reduced the expression of the c proteins related to cuproptosis DLAT, FDX1, LIAS and ACO2 (Figure 6B). These results confirmed that Y_2O_3 NPs induce cuproptosis in neurons.

ATP7A Mediates the Disruption of Copper Output Induced by Yttrium Oxide Nanoparticles

To investigate the mechanism of Y_2O_3 NP-induced copper accumulation in neuronal cells, we utilized RT–qPCR to detect mRNA levels of key Cu transport genes, including the copper uptake proteins copper transporter 1 (CTR1) and divalent metal transporter 1 (DMT1) and the Cu output protein ATP7A (Figure 7A). These results revealed that Y_2O_3 NPs decreased the expression of ATP7A in PC12 cells but had no significant effect on the expression of the Cu input proteins CTR1 and DMT1. ATP7A is located at the plasma membrane and Golgi apparatus and is responsible for transporting Cu ions from the intracellular to the extracellular space and regulating cellular copper homeostasis. Western blot analysis and IF analysis demonstrated that Y_2O_3 NPs reduced ATP7A protein expression in PC12 cells (Figure 7B and C). Since the 100 mg/kg Y_2O_3 NP group was the lowest dose group in which significant cuproptosis in the cerebral cortex occurred, we assessed the protein expression of ATP7A in the 100 mg/kg Y_2O_3 NP group. Western blot analysis and IHC staining revealed that Y_2O_3 NPs downregulated the expression level of ATP7A in the 100 mg/kg Y_2O_3 NP group (Figure 7D and E).

We subsequently transfected PC12 cells with plasmids that overexpress ATP7A to test the hypothesis that ATP7A mediates Y_2O_3 NP-induced cuproptosis. The results of the CCK8 experiment indicated that ATP7A overexpression had

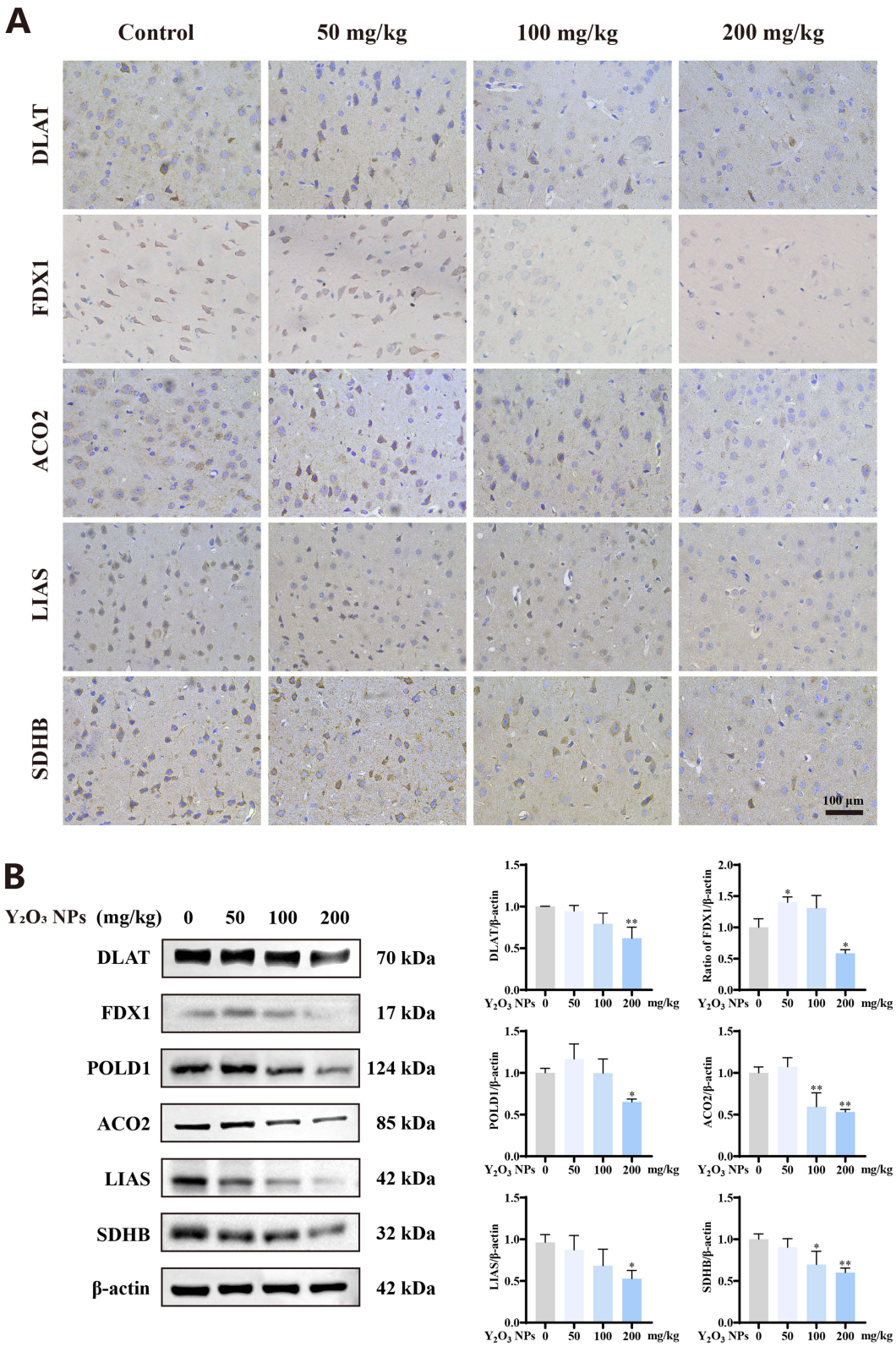

Figure 4 Y_2O_3 NPs induce cuproptosis in the rat cerebral cortex. (**A**) IHC staining of DLAT and Fe-S cluster proteins (FDX1, ACO2, LIAS, and SDHB) in the rat cerebral cortex after exposure to Y_2O_3 NPs. (**B**) Western blot and quantification of DLAT and Fe-S cluster proteins (POLD1, FDX1, ACO2, LIAS, and SDHB) in rat cerebral cortex cells after exposure to Y_2O_3 NPs. The results are shown as the means ± SDs. **P*<0.05 and ***P*<0.01.

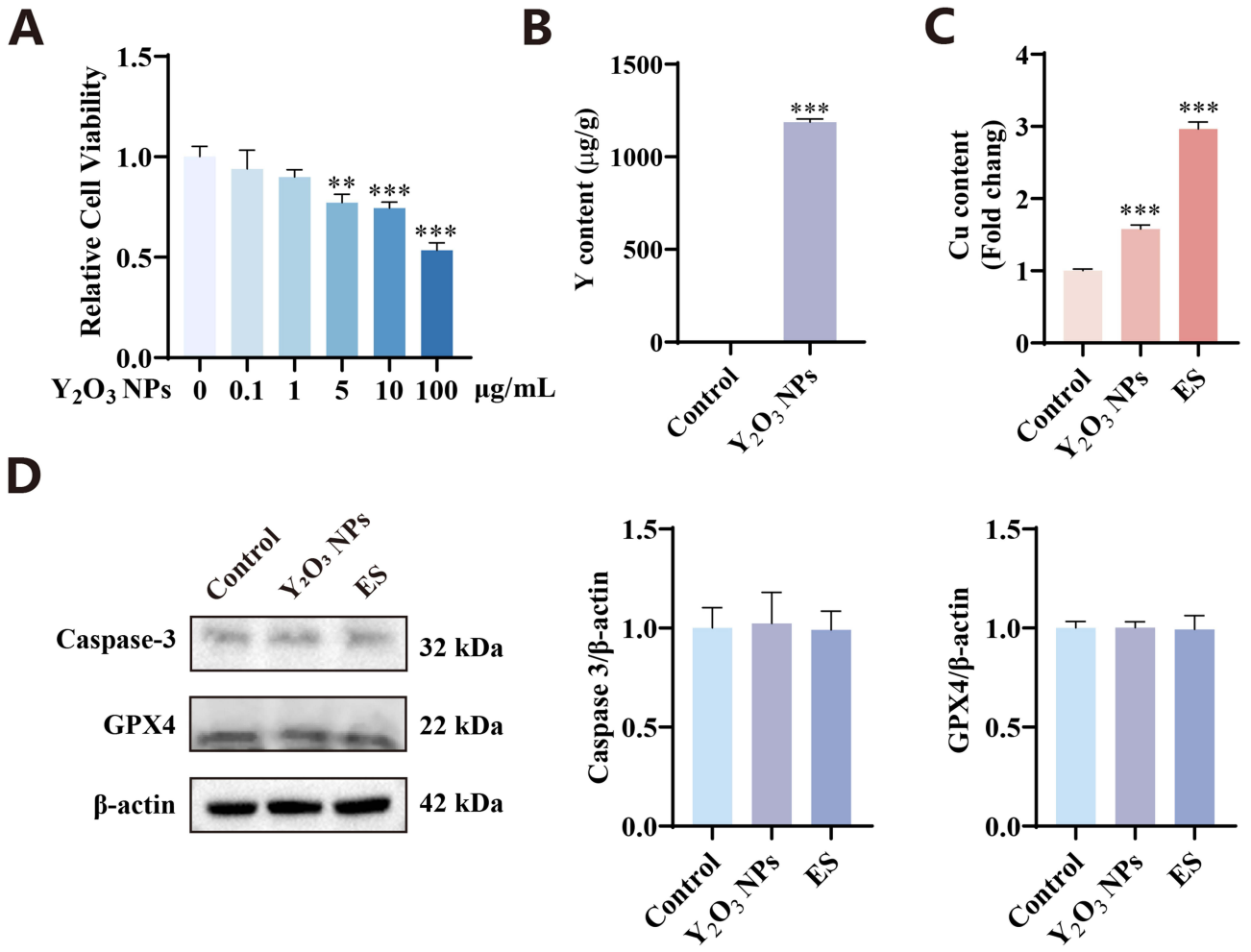

Figure 5 Y_2O_3 NPs induce neuronal cell death in vitro. (**A**) Viability of PC12 cells after a 24-hour treatment with Y_2O_3 NPs. (**B**) Y content in PC12 cells after treatment with Y_2O_3 NPs. (**C**) Cu content in PC12 cells treated with Y_2O_3 NPs or ES. (**D**) Western blot analysis and quantification of Caspase-3 and CPX4 in PC12 cells after treatment with Y_2O_3 NPs or ES. The results are shown as the means ± SDs. $^{**}P<0.01$ and $^{***}P<0.001$.

no significant effect on the viability of PC12 cells but did ameliorate the decrease in viability caused by Y_2O_3 NPs (Figure 8A). ATP7A overexpression reversed the Y_2O_3 NP-induced accumulation of intracellular Cu, indicating that ATP7A affects Cu output disorder and leads to an imbalance in copper homeostasis in neuronal cells (Figure 8B). Protein expression analysis of DLAT and Fe-S cluster proteins (FDX1, POLD1, ACO2, LIAS and SDHB) revealed that ATP7A overexpression alleviated Y_2O_3 NP-induced cuproptosis in PC12 cells (Figure 8C). These findings indicate that Y_2O_3 NPs disrupt Cu output and dysregulate Cu homeostasis by reducing ATP7A expression, ultimately inducing cuproptosis in neuronal cells.

Discussion

In this study, we reported that exposure to Y_2O_3 NPs led to cognitive and memory impairment in rats. The medial temporal lobe of the cerebral cortex is responsible for long-term declarative memory and advanced perceptual processing[15,16] and is particularly important for spatial navigation and memory behaviour.[17] Studies have shown that medial temporal lobe atrophy affects the spatial navigation ability of older adults.[18] The results of the MWM test revealed that Y_2O_3 NPs led to a decrease in spatial navigation and memory abilities in rats. These findings suggest that the cognitive memory impairment caused by Y_2O_3 NPs may be due to damage to the cerebral cortex. Neuronal cells are distributed mainly in the cerebral cortex and are the basic functional units of the brain. Neuronal cells form neural networks through synaptic connections, and their synaptic plasticity is the cellular basis for learning and memory.[19] We

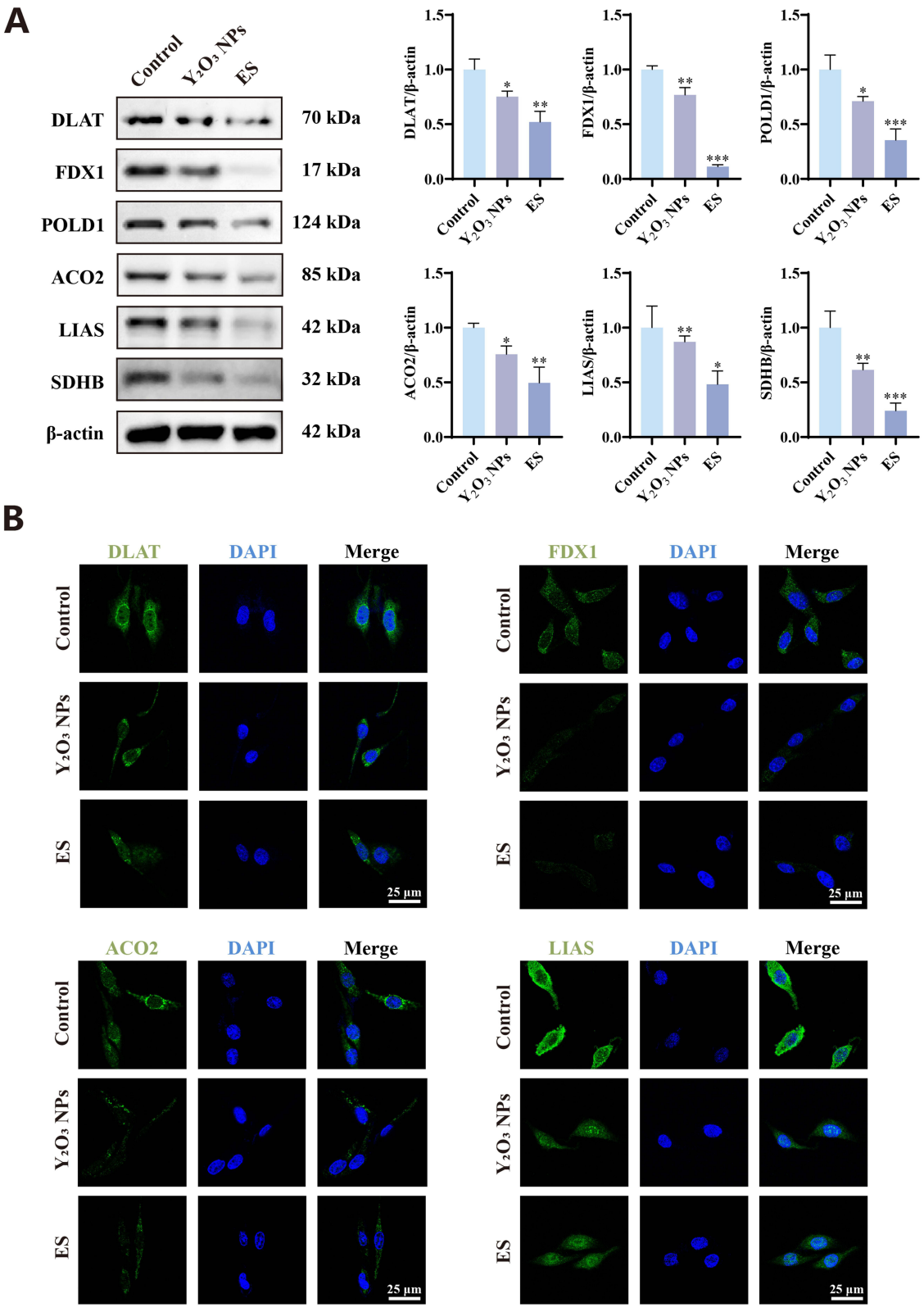

Figure 6 Y_2O_3 NPs induce cuproptosis in neuronal cells in vitro. (**A**) Western blot analysis and quantification of DLAT and Fe-S cluster proteins (FDX1, POLD1, ACO2, LIAS, and SDHB) in PC12 cells after treatment with Y_2O_3 NPs or ES. (**B**) IF analysis of DLAT and Fe–S cluster proteins (FDX1, ACO2, and LIAS) in PC12 cells after treatment with Y_2O_3 NPs or ES. The results are shown as the means ± SDs. * P<0.05, ** P<0.01 and *** P<0.001.

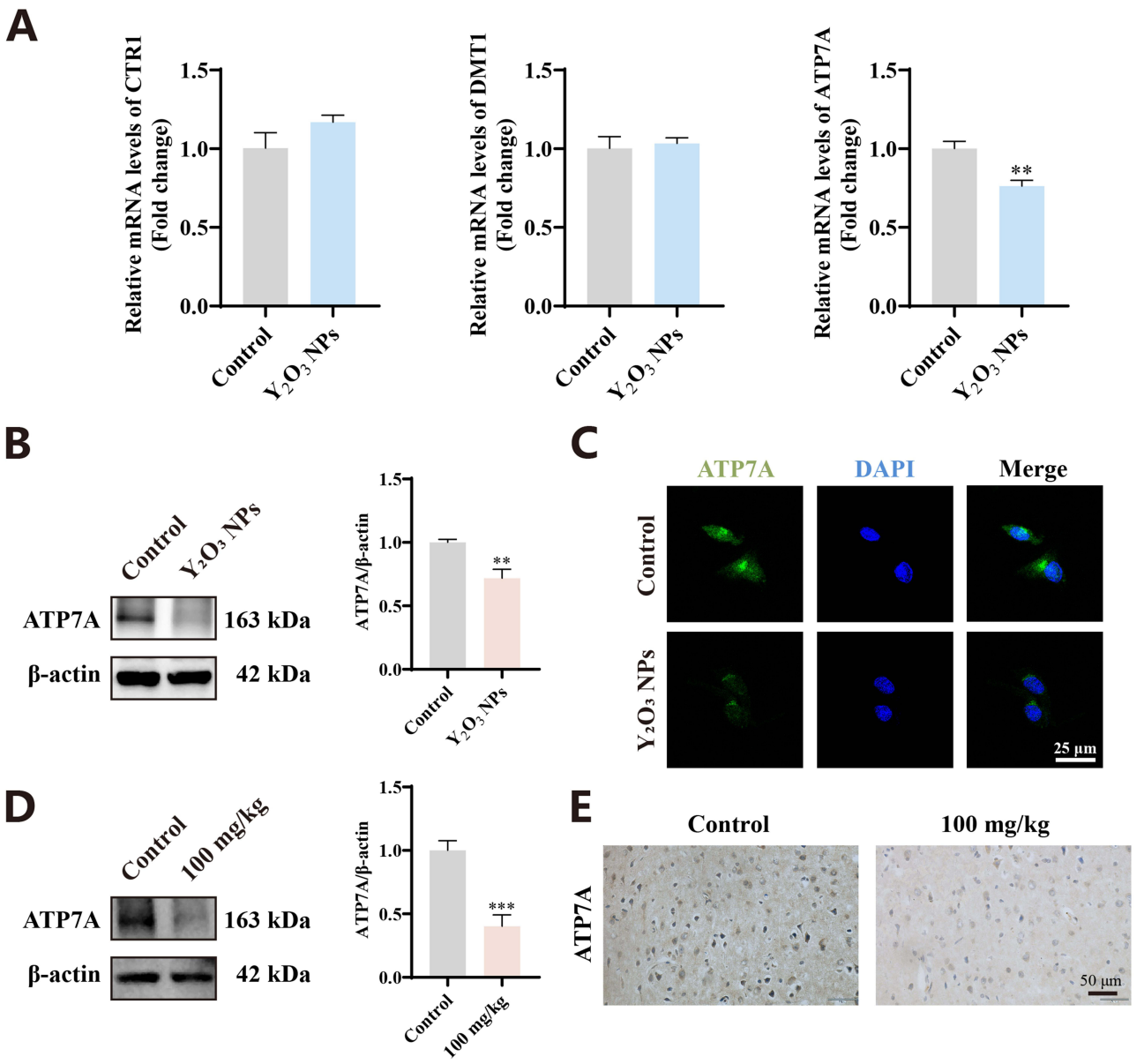

Figure 7 Mechanism by which Y_2O_3 NPs induce neuronal cell cuproptosis. (**A**) RT–qPCR analysis of CTR1, DMT1 and ATP7A expression in PC12 cells after treatment with Y_2O_3 NPs. (**B**) Western blot analysis of ATP7A expression in PC12 cells after treatment with Y_2O_3 NPs. (**C**) IF staining of ATP7A in PC12 cells after treatment with Y_2O_3 NPs. (**D**) Western blot analysis of ATP7A expression in the rat cerebral cortex after exposure to Y_2O_3 NPs. (**E**) IHC staining of ATP7A in the rat cerebral cortex after exposure to Y_2O_3 NPs. The results are shown as the means ± SDs. $^{**}P < 0.01$ and $^{***}P < 0.001$.

found through histological analysis that Y_2O_3 NPs cause neuronal cell death and significantly decrease the number of cortical neurons. Therefore, Y_2O_3 NPs induce neuronal cell death in the cerebral cortex, leading to impaired cognitive memory function.

Cu is an important component of neuronal synaptic transmission, with a concentration of approximately 30 μM in the synaptic cleft.[20] During neuronal excitation, free Cu is released from vesicles into the synaptic cleft.[21] Secreted Cu combines with several neurotransmitters to regulate neurotransmission and neuronal excitability.[22] Cu homeostasis disorders are associated with cognitive decline in neurodegenerative diseases, such as Huntington's disease and Alzheimer's disease.[23] A cross-sectional study revealed that individuals with high serum Cu levels have a significantly greater incidence of depression.[24] Recent studies have shown a significant correlation between cognitive impairment and hippocampal atrophy with elevated levels of Cu.[25] Metal exposure may disrupt copper homeostasis within cells. For

https://doi.org/10.2147/IJN.S515951

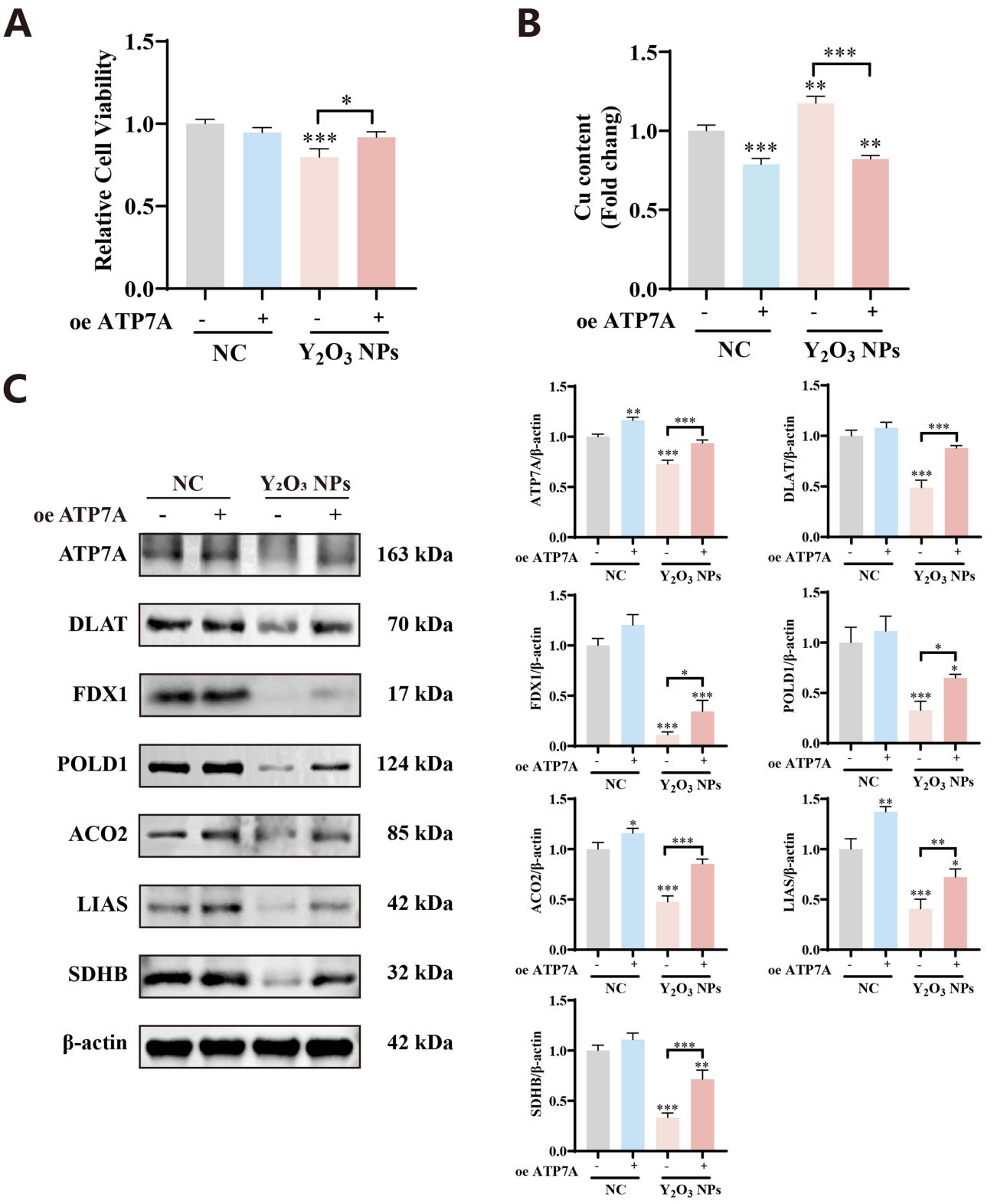

Figure 8 ATP7A mediates copper output disorder induced by Y_2O_3 NPs. (**A**) Viability of PC12 cells after ATP7A overexpression. (**B**) Cu content in PC12 cells after ATP7A overexpression. (**C**) Western blot and quantification analysis of ATP7A, DLAT and Fe-S cluster proteins (FDX1, POLD1, ACO2, LIAS, and SDHB) in PC12 cells after ATP7A overexpression. The results are shown as the means ± SDs. **P*<0.05, ***P*<0.01, and ****P*<0.001.

example, Pb exposure leads to mitochondrial Cu overload in microglia, exacerbating the pathology of Alzheimer's disease.[26] Our results indicate that exposure to Y_2O_3 NPs leads to an increase in the Cu content in the cerebral cortex and neuronal cells. Excessive copper accumulation in the brain can lead to cuproptosis. Our findings indicate that the main mechanism by which Y_2O_3 NPs induce neuronal cell death is not apoptosis or ferroptosis. Cuproptosis is a newly identified form of cell death distinct from apoptosis. Excessive Cu^{2+} is reduced to Cu^{+} by FDX1 in mitochondria. Cu^{+} binding with mitochondrial tricarboxylic acid cycle components leads to the reduced synthesis of Fe–S cluster proteins and oligomerization of DLAT, resulting in protein toxicity stress and cuproptosis.[27] Cells that rely heavily on mitochondrial respiration to generate energy are most susceptible to copper metabolism and cuproptosis.[28] Neuronal cells rely on aerobic respiration to obtain energy and maintain normal function and are susceptible to Cu homeostasis disorders.[29] Therefore, we speculate that Y_2O_3 NPs may induce cuproptosis in neuronal cells. We analysed the expression of proteins related to cuproptosis in neuronal cells both in vivo and in vitro and found that Y_2O_3 NPs reduced the expression levels of DLAT and Fe-S cluster proteins. These findings indicate that Y_2O_3 NPs induce cuproptosis in neuronal cells.

We investigated the potential mechanism by which Y_2O_3 NPs lead to intracellular copper accumulation. Intracellular copper homeostasis is strictly regulated. CTR1 and DMT1 are Cu transport proteins located on the plasma membrane and are responsible for transporting Cu to the cytoplasm.[30] Previous studies have shown that exposure to metallic manganese leads to intracellular copper overload by upregulating CTR1 expression.[31] The ATF3/SPI1/CTR1 signalling pathway mediates cuproptosis induced by advanced glycosylation end products in myocardial injury in diabetes.[32] Our results indicate that Y_2O_3 NPs do not significantly alter the mRNA expression of the copper input proteins CTR1 and DMT1 but significantly reduce the expression of ATP7A. The Cu transporter ATP7A is a Cu ATPase whose expression is significantly upregulated in differentiated neurons.[29] When the intracellular Cu content is too high, ATP7A is transferred from the Golgi apparatus to the cytoplasm, where it forms vesicles to expel excess Cu. ATP7A functional defects can damage the nervous system, leading to the occurrence of Menkes disease.[33] Previous studies have shown that a decrease in ATP7A mRNA expression is significantly correlated with an increase in ceruloplasmin levels and neuronal metabolic disorders and is closely related to the occurrence of depression.[34] Therefore, we hypothesize that the decrease in ATP7A expression caused by Y_2O_3 NPs leads to a decrease in copper efflux ability in neuronal cells and demonstrated through in vitro recovery experiments that Y_2O_3 NPs induce Cu accumulation and cuproptosis by reducing ATP7A expression.

The mechanism by which Y_2O_3 NPs lead to decreased ATP7A protein expression is not yet clear. ATP7A and ATP7B are different subtypes of ATPases with similar protein structures.[35] ATP7B is expressed mainly in the liver. The localization, expression and function of ATP7B in the brain are not as good as those of ATP7A. The two have different functions. ATP7A has a homeostatic effect on maintaining the intracellular Cu content, whereas ATP7B performs a biosynthetic function of delivering Cu to enzymes, including ceruloplasmin.[36] Previous studies have shown that exposure to metallic lead promotes the degradation of ATP7B and interferes with copper output by increasing copper metabolism MURR1 domain (COMMD1) protein levels.[37] Therefore, we speculate that Y_2O_3 NPs may lead to a decrease in ATP7A expression by promoting the degradation of the ATP7A protein. Apolipoprotein J (Clusterin) and COMMD1 can regulate the degradation of the mammalian Cu ATP7A and ATP7B ATPases.[38] COMMD1 acts as a subunit of the ATP7A ubiquitin ligase containing Cul2, promoting the degradation of the ATP7A protein through the proteasome pathway.[39] In addition, recent studies have shown that caveolin-1 (Cav-1) also regulates the degradation of ATP7A. Cav-1 is a scaffold protein that can bind to ATP7A through its scaffold domain, preventing ATP7A ubiquitination and proteasomal degradation. The binding of Cav-1 and ATP7A may also limit the recruitment of COMMD1 to ATP7A, preventing its degradation.[40] However, whether Y_2O_3 NPs regulate ATP7A degradation through the aforementioned molecules remains to be proven.

For the first time, in this study, we found that Y_2O_3 NPs mediate cuproptosis in neuronal cells, leading to cognitive memory dysfunction, and demonstrated the role of copper output impairment caused by decreased ATP7A expression in Y_2O_3 NP-induced copper homeostasis disorders. These findings suggest that the neurotoxicity of Y_2O_3 NPs can be prevented by restoring normal copper output and provide a basis for the treatment of neurotoxicity.

Conclusions

This study revealed that Y_2O_3 NPs mediate cuproptosis in neuronal cells, leading to cognitive memory dysfunction in a rat model. In terms of the mechanism, this study further demonstrated the role of copper output impairment caused by decreased ATP7A expression in Y_2O_3 NP-induced copper homeostasis disorders, providing a solution to mitigate the neurotoxicity of Y_2O_3 NPs. These findings provide valuable insights for better understanding the neurotoxicity of Y_2O_3 NPs and contribute to the safe application of Y_2O_3 NPs in the biomedical field.

Acknowledgments

This work was supported by the National Natural Science Fund (grant number: 81600904) and the Guangzhou Science and Technology Plan Project Jointly Funded by City and Universities (grant number: 2023A03J0328).

Disclosure

The authors report no conflicts of interest in this work.

References

1. Pérez Palmer N, Trejo Ortega B, Joshi P. Cognitive impairment in older adults: epidemiology, diagnosis, and treatment. *Psychiatr Clin North Am*. 2022;45(4):639–661. doi:10.1016/j.psc.2022.07.010
2. Yang S, Lee S, Lee Y, et al. Cationic nanoplastic causes mitochondrial dysfunction in neural progenitor cells and impairs hippocampal neurogenesis. *Free Radic Biol Med*. 2023;208:194–210. doi:10.1016/j.freeradbiomed.2023.08.010
3. Sharma A, Feng L, Muresanu DF, et al. Manganese nanoparticles induce blood-brain barrier disruption, cerebral blood flow reduction, edema formation and brain pathology associated with cognitive and motor dysfunctions. *Prog Brain Res*. 2021;265:385–406. doi:10.1016/bs.pbr.2021.06.015
4. Lei P, Ayton S, Bush AI. The essential elements of Alzheimer's disease. *J Biol Chem*. 2021;296:100105. doi:10.1074/jbc.REV120.008207
5. Chen LL, Fan YG, Zhao LX, Zhang Q, Wang ZY. The metal ion hypothesis of Alzheimer's disease and the anti-neuroinflammatory effect of metal chelators. *Bioorg Chem*. 2023;131:106301. doi:10.1016/j.bioorg.2022.106301
6. Lin C, Liu G, Huang Y, Liu S, Tang B. Rare-earth nanoparticles induce depression, anxiety-like behavior, and memory impairment in mice. *Food Chem Toxicolo*. 2021;156:112442. doi:10.1016/j.fct.2021.112442
7. Yu X, Cao X, Yue L, et al. Phosphate induced surface transformation alleviated the cytotoxicity of Y(2)O(3) nanoparticles to tobacco BY-2 cells. *Sci Total Environ*. 2020;732:139276. doi:10.1016/j.scitotenv.2020.139276
8. Panyala A, Chinde S, Kumari SI, Grover P. Assessment of genotoxicity and biodistribution of nano- and micron-sized yttrium oxide in rats after acute oral treatment. *J Appl Toxicol*. 2017;37(12):1379–1395. doi:10.1002/jat.3505
9. Andelman T, Gordonov S, Busto G, Moghe PV, Riman RE. Synthesis and cytotoxicity of Y(2)O(3) nanoparticles of various morphologies. *Nanoscale Res Lett*. 2009;5(2):263–273. doi:10.1007/s11671-009-9445-0
10. Selvaraj V, Bodapati S, Murray E, et al. Cytotoxicity and genotoxicity caused by yttrium oxide nanoparticles in HEK293 cells. *Int J Nanomedicine*. 2014;9:1379–1391. doi:10.2147/IJN.S52625
11. Gao C, Jin Y, Jia G, et al. Y(2)O(3) nanoparticles caused bone tissue damage by breaking the intracellular phosphate balance in bone marrow stromal cells. *ACS Nano*. 2019;13(1):313–323. doi:10.1021/acsnano.8b06211
12. Ding Y, Tian Y, Zeng Z, et al. YCl(3) promotes neuronal cell death by inducing apoptotic pathways in rats. *Biomed Res Int*. 2017;2017:2183658. doi:10.1155/2017/2183658
13. Sayour H, Kassem S, Canfarotta F, Czulak J, Mohamed M, Piletsky S. Biocompatibility and biodistribution of surface-modified yttrium oxide nanoparticles for potential theranostic applications. *Environ Sci Pollut Res Int*. 2020;27(16):19095–19107. doi:10.1007/s11356-019-04309-9
14. Panyala A, Chinde S, Kumari SI, et al. Comparative study of toxicological assessment of yttrium oxide nano- and microparticles in Wistar rats after 28 days of repeated oral administration. *Mutagenesis*. 2019;34(2):181–201. doi:10.1093/mutage/gey044
15. Martin CB, Barense MD. Perception and memory in the ventral visual stream and medial temporal lobe. *Ann Rev Vision Sci*. 2023;9(1):409–434. doi:10.1146/annurev-vision-120222-014200
16. Hannula DE, Minor GN, Slabbekoorn D. Conscious awareness and memory systems in the brain. *Wiley Interdiscip Rev Cogn Sci*. 2023;14(5):e1648. doi:10.1002/wcs.1648
17. Donoghue T, Cao R, Han CZ, et al. Single neurons in the human medial temporal lobe flexibly shift representations across spatial and memory tasks. *Hippocampus*. 2023;33(5):600–615. doi:10.1002/hipo.23539
18. Pawlaczyk NA, Milner R, Szmytke M, et al. Medial temporal lobe atrophy in older adults with subjective cognitive impairments affects gait parameters in the spatial navigation task. *J Aging Phys Act*. 2024;32(2):185–197. doi:10.1123/japa.2022-0335
19. Huang YS, Mendez R, Fernandez M, Richter JD. CPEB and translational control by cytoplasmic polyadenylation: impact on synaptic plasticity, learning, and memory. *mol Psychiatry*. 2023;28(7):2728–2736. doi:10.1038/s41380-023-02088-x
20. Kim N, Lee HJ. Redox-active metal ions and amyloid-degrading enzymes in alzheimer's disease. *Int J mol Sci*. 2021;22(14). doi:10.3390/ijms22147697
21. Kawahara M, Tanaka KI, Kato-Negishi M. Copper as a collaborative partner of zinc-induced neurotoxicity in the pathogenesis of vascular dementia. *Int J mol Sci*. 2021;22(14):7242. doi:10.3390/ijms22147242
22. Wang L, Yin YL, Liu XZ, et al. Current understanding of metal ions in the pathogenesis of alzheimer's disease. *Transl Neurodegener*. 2020;9:10. doi:10.1186/s40035-020-00189-z

23. Feng D, Zhao Y, Li W, Li X, Wan J, Wang F. Copper neurotoxicity: induction of cognitive dysfunction: a review. *Medicine*. 2023;102(48):e36375. doi:10.1097/md.0000000000036375
24. Hongrong W, Qingqi L, Rong G, Shuangyang T, Kaifang Z, Jianfeng Z. BMI modifies the association between depression symptoms and serum copper levels. *Biol Trace Elem Res*. 2023;201(9):4216–4229. doi:10.1007/s12011-022-03505-y
25. Philbert SA, Schönberger SJ, Xu J, Church SJ, Unwin RD, Cooper GJS. Elevated hippocampal copper in cases of type 2 diabetes. *EBioMedicine*. 2022;86:104317. doi:10.1016/j.ebiom.2022.104317
26. Huang D, Chen L, Ji Q, et al. Lead aggravates Alzheimer's disease pathology via mitochondrial copper accumulation regulated by COX17. *Redox Biol*. 2024;69:102990. doi:10.1016/j.redox.2023.102990
27. Duan WJ, He RR. Cuproptosis: copper-induced regulated cell death. *Sci China Life Sci*. 2022;65(8):1680–1682. doi:10.1007/s11427-022-2106-6
28. Tsvetkov P, Coy S, Petrova B, et al. Copper induces cell death by targeting lipoylated TCA cycle proteins. *Science*. 2022;375(6586):1254–1261. doi:10.1126/science.abf0529
29. Gale J, Aizenman E. The physiological and pathophysiological roles of copper in the nervous system. *Eur J Neurosci*. 2024;60(1):3505–3543. doi:10.1111/ejn.16370
30. Bhattacharjee A, Ghosh S, Chatterji A, Chakraborty K. Neuron-glia: understanding cellular copper homeostasis, its cross-talk and their contribution towards neurodegenerative diseases. *Metallomics*. 2020;12(12):1897–1911. doi:10.1039/d0mt00168f
31. Zheng G, Chen J, Zheng W. Relative contribution of CTR1 and DMT1 in copper transport by the blood-CSF barrier: implication in manganese-induced neurotoxicity. *Toxicol Appl Pharmacol*. 2012;260(3):285–293. doi:10.1016/j.taap.2012.03.006
32. Huo S, Wang Q, Shi W, et al. ATF3/SPI1/SLC31A1 signaling promotes cuproptosis induced by advanced glycosylation end products in diabetic myocardial injury. *Int J Mol Sci*. 2023;24(2):1667. doi:10.3390/ijms24021667
33. Horn N, Wittung-Stafshede P. ATP7A-regulated enzyme metalation and trafficking in the Menkes disease puzzle. *Biomedicines*. 2021;9(4):391. doi:10.3390/biomedicines9040391
34. Liu X, Zhong S, Yan L, et al. Correlations among mRNA expression levels of ATP7A, serum ceruloplasmin levels, and neuronal metabolism in unmedicated major depressive disorder. *Int J Neuropsychopharmacol*. 2020;23(10):642–652. doi:10.1093/ijnp/pyaa038
35. Zhou Y, Zhang L. The interplay between copper metabolism and microbes: in perspective of host copper-dependent ATPases ATP7A/B. *Front Cellular Infect Microbiol*. 2023;13. doi:10.3389/fcimb.2023.1267931
36. La Fontaine S, Ackland ML, Mercer JFB. Mammalian copper-transporting P-type ATPases, ATP7A and ATP7B: emerging roles. *Int J Biochem Cell Biol*. 2010;42(2):206–209. doi:10.1016/j.biocel.2009.11.007
37. Liu Y, Zhao Z-H, Wang T, et al. Lead exposure disturbs ATP7B-mediated copper export from brain barrier cells by inhibiting XIAP-regulated COMMD1 protein degradation. *Ecotoxicol Environ Saf*. 2023;256:114861. doi:10.1016/j.ecoenv.2023.114861
38. Materia S, Cater MA, Klomp LW, Mercer JF, La Fontaine S. Clusterin (apolipoprotein J), a molecular chaperone that facilitates degradation of the copper-ATPases ATP7A and ATP7B. *J Biol Chem*. 2011;286(12):10073–10083. doi:10.1074/jbc.M110.190546
39. Materia S, Cater MA, Klomp LW, Mercer JF, La Fontaine S. Clusterin and COMMD1 independently regulate degradation of the mammalian copper ATPases ATP7A and ATP7B. *J Biol Chem*. 2012;287(4):2485–2499. doi:10.1074/jbc.M111.302216
40. Sudhahar V, Okur MN, O'Bryan JP, et al. Caveolin-1 stabilizes ATP7A, a copper transporter for extracellular SOD, in vascular tissue to maintain endothelial function. *Am J Physiol Cell Physiol*. 2020;319(5):C933–c944. doi:10.1152/ajpcell.00151.2020